and $Q_0 = 1/(2|\delta_k|)$, which can be shown that the critical points in this case are those located at $\mathrm{Re}(Z_l) = \mathrm{Im}(Z_l)$, and this corresponds exactly to the argument developed in [1], [5]. Here, we may name $|x|$ as the *modification factor of critical-points bandwidth.* Usually, this factor is close to one and can be ignored in most cases [7]. For the sake of measurement, we can avail ourselves of the vector network analyzer to measure input impedance in the sweep-frequency operation mode, then mark the *critical-points frequencies* f_1 and f_2 in which the corresponding *reactance* is maximum in f_1 or f_2 and minimum *vice versa* only within the impedance locus, and finally mark the *detuned crossover frequencies* f_3 and f_4 in which the corresponding *impedance* is identical with crossover point. Thus, Q_0 can be estimated from (15). Moreover, even the simpler (16) is accurate enough in most cases. For the measured admittance locus near the *detuned-open point*, which is electrical coupling predominantly, the second-Foster type equivalent circuit such as Fig. 1(b) can be used. Follow the same derivation process as mentioned above. However, the *impedance* locus and parameters are changed to the *admittance* locus and parameters for the *dual* expression, respectively. Similar results can be developed and the *inverted* Smith Chart can be used for measurement.

IV. Experimental Results

To illustrate the principle and procedure, two types of resonators, dielectric resonator and metal cavity, were measured. In the case of the overcoupled dielectric resonator, the measured input impedance is shown in Fig. 3(a) and the frequencies for critical points and detuned crossover point are: f_1 =7.0279 GHz, f_2 =7.0292 GHz, f_3 =7.0123 GHz, and f_4 =7.0473 GHz, respectively. Thus, Q_0 =5392 is estimated from (15), Q_0 =5407 from (16), and $|x|$ =0.997 from (12). These estimated Q_0 corresponds to the result of Kajfez's method, which gets $Q_0 \approx$5400, and the difference can be negligible if measured error is considered. Fig. 3(b) is the measured result with the identical dielectric resonator but in the undercoupled condition, and in this case f_1 =7.0397 GHz, f_2 =7.0410 GHz, f_3 =7.0329 GHz, and f_4 =7.0500 GHz, thus Q_0 =5353 or Q_0 =5416 and $|x|$ =0.988 are estimated from (15), (16), and (12), respectively. The resultant $Q_0 \approx$5400 is nearly identical with the overcoupled result if measured error is considered and ignored. Fig. 4(a) and (b) are the measurement plots for the cases of the same metal cavity under overcoupled and undercoupled conditions, respectively. Again, both results get $Q_0 \approx$2600 by *critical-points method* with the inverted Smith Chart, and the small difference can be neglected in practice. Also note that the *modification factor of critical-points bandwidth* is $|x|$ =0.937 and the deviation error of Q_0 between (15) and (16) is less than 7% even for the case of *weak undercoupled* shown in Fig. 4(b).

V. Conclusion

The principle and measurement procedure described in this paper result in the *critical-points method.* As far as the four-frequency measurement is concerned, four frequencies of three points need measuring; that is, two *critical-points* frequencies and two *detuned crossover* frequencies on the Smith chart (impedance or inverted admittance). The unloaded quality Q_0 can be estimated from (15) quickly and accurately without any subtle discrimination between lossy and lossless, undercoupled, and overcoupled cases. As far as the two-frequency measurement is concerned, only two frequencies of two critical points need measuring. From (16), it is worth pointing out that *the unloaded Q_0 could be measured and evaluated in reflection mode as easily as its counterpart the loaded Q_L in transmission mode* (i.e., *half-power points' method*). This conclusion stands to reason in most cases as long as practical errors are ignored. Thus, only two *critical-points* frequencies and (16) need to be measured and applied without any additional information such as coupling coefficients to be measured or any auxiliary tool such as transparent Smith chart template required for the determination of Q_0, which significantly simplifies the job of Q_0 measurement.

Acknowledgment

The authors are much indebted to K. S. Chin for his assistance in the measurement of the data and to Dr. T. I. Hou for his generosity with providing the test samples as well.

References

[1] E. L. Ginzton, *Microwave Measurements,* ch. 9, pp. 391–431, 1957.
[2] M. Sucher and J. Fox, *Handbook of Microwave Measurements*, 3rd ed., vol. II, pp. 417–491, 1963.
[3] D. Kajfez and E. J. Hwan, "Q-factor measurement with network analyzer," *IEEE Trans. Microwave Theory Tech.*, vol. MTT-32, no. 7, pp. 666–670, 1984.
[4] S. Ramo, J. R. Whinnery, and T. V. Duzer, *Fields and Waves in Communication Electronics*, 2nd ed. 1984, pp. 558–562.
[5] ——, pp. 509–512.
[6] C. R. Wylie and L. C. Barrett, *Advanced Engineering Mathematics*, 5th ed. 1982, p. 988.
[7] E.-Y. Sun, "Q measurement of microwave dielectric resonators," *Technique Report in CSIST*, 1994.

Further Analysis of Open-Ended Dielectric Sensors

M. Okoniewski, J. Anderson, E. Okoniewska,
K. Caputa, and S. S. Stuchly

***Abstract*—The effect on the input reflection coefficient of the dimensions of open-ended coaxial lines is investigated. Using a standard FDTD technique, the effects of variations in the flange and conductor dimensions on the reflection coefficient of a 3.6 mm coaxial line immersed in water or methanol are simulated. Simulation results are compared with measurements and previous moment method calculations. It is found that the presence or absence of a flange affects the input reflection coefficient substantially in some cases. The results also show that inversion formulas developed for lines with infinite flanges are not valid for flanges with finite radii.**

I. Introduction

An open-ended coaxial line immersed in or pressed against an unknown dielectric can serve as a dielectric sensor [1]–[3]. Inversion formulas giving the permittivity as a function of the measured reflection coefficient are required for this application. Such formulas are constructed using multiple numerical simulation results. An idealized sensor with an assumed infinite flange and inner and outer conductor inner radii corresponding to a characteristic impedance of precisely 50 Ω was previously analyzed using the moment method

Manuscript received July 19, 1994; revised April 24, 1995.
The authors are with the Department of Electrical and Computer Engineering, University of Victoria, Victoria, BC V8W 3P6, Canada.
IEEE Log Number 9412673.

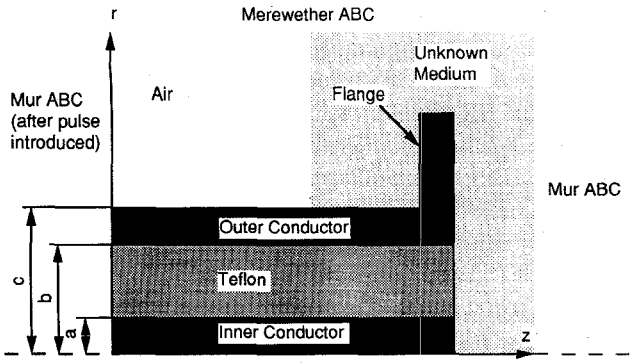

Fig. 1. Schematic presentation of the coaxial sensor: $a = 0.456$ mm—inner conductor radius; $b = 1.49$ mm—outer conductor inner radius; $c = 1.8$ mm—outer conductor outer radius.

[4], [5]. Deviations in the sensor from its idealized dimensions reduce the accuracy of the inversion formula and are the subject of this investigation.

A detailed analysis of the dielectric sensor is necessary because network analyzer calibration standards cannot be attached directly to its open end. The network analyzer and sensor can be calibrated using reference liquids but the accuracy of this technique is limited by the uncertainty in the dielectric properties of the reference liquids and their sensitivity to temperature changes [3]. Potentially greater accuracy is possible by characterizing the sensor in detail, attaching it to a pre-calibrated network analyzer, and compensating for its internal reflections, attenuation, and electrical length with time domain gating and normalization [1]. The moment method analysis previously performed assumed an infinite flange and did not account for mechanical tolerances in inner and outer conductor probe radii.

In this investigation, a 3.6-mm outer diameter dielectric sensor immersed in water or in methanol is modeled using a standard FDTD technique [6]–[10], which is particularly suitable for problems in which the geometry must be specified at run time. The effects of the finite flange and geometric imperfections on the measured reflection coefficient are computed and compared with experimental results. Such an analysis is a necessary precursor to a rigorous error analysis of the inversion formula, to the calculation of correction coefficients (derivatives with respect to probe imperfections), and to evaluations of sensor modifications and designs. Computing different inversion formulas to account for the different types of sensor imperfections would not be practical.

II. Method of Calculation

A 2-D, cylindrical coordinate FDTD code for the geometry depicted in Fig. 1 was used. The singularity in the coordinate system along the z-axis was handled with techniques described in [6] and [11]. Field components at the aperture of the sensor were computed using constitutive parameters averaged between the two media. The coaxial line was excited by specifying the values of the TEM mode radial electric field on the boundary of the problem space (The line $z = 0$ in Fig. 1). The time envelope of the excitation was a gated Gaussian pulse so that the exciting field vanished before reflections from the end of the line returned to the excitation plane. A first-order Mur absorbing boundary condition was used at the excitation plane after the gate was switched off [12]. A Merewether ABC was applied at the radial boundary of the problem space [13]. The remaining boundary of the problem space was also terminated with a first order Mur ABC.

The reflection coefficient was computed from the time series of the electric and magnetic fields observed at a sampling point. In the FDTD mesh the electric and magnetic fields are offset and are computed at different times. Therefore, interpolation in space and time was used to obtain the field values at the sampling point, after which the quantities were transformed into the frequency domain—allowing the wave impedance and the reflection coefficient to be calculated—using a technique described in [14].

Several problem discretizations were tested. The problem space was up to 70 mm long and 15 mm in radius. The densest FDTD mesh had 700 axial and 150 radial units and was simulated for up to 5600 time steps. The longest execution time was 30 min. on an HP 730 computer. To simulate an infinite flange with FDTD, the program was halted immediately after the first reflected pulse had reached negligible values.

TABLE I
Reflection Coefficient for a Dielectric Sensor with Infinite Flange Computed Using Method of Moments and FDTD

Freq [GHz]	Reflection Coeff.					
	Water			Methanol		
	MoM	FDTD	Δ [%]	MoM	FDTD	Δ [%]
2.117	0.8806	0.8792	0.16	0.7202	0.7208	-0.08
5.098	0.7759	0.7812	-0.68	0.4939	0.4954	-0.30
10.07	0.7164	0.7221	-0.79	0.4007	0.4004	0.08

III. Results

A section of a 3.6-mm outer diameter coaxial line immersed in water and methanol was simulated. The simulated line was sufficiently long to allow the excitation pulse to be introduced before reflections returned to the excitation plane and to allow a field sampling point to be located far enough from the end of the line for the higher order modes to decay. The FDTD code did not incorporate routines to account for dispersive media, which were handled using separate program runs with previously reported constitutive parameters corresponding to the frequencies of interest [1], [4]. Measurements corresponding to selected cases were made using a HP8720 network analyzer and techniques previously reported [1].

Table I compares two methods of simulating the reflection coefficient of a sensor with an infinite flange immersed in water and methanol: the moment method and the FDTD technique. The computations were made at frequencies of 2.117, 5.098, and 10.07 GHz. As expected the two numerical techniques give close results. Differences were likely the result of the manner in which the FDTD code treated the discontinuities in constitutive parameters at the aperture.

Fig. 2 shows measured and computed reflection coefficients as the flange radius varies from the minimum to largest considered value, for a sensor immersed in water at 2.117, 5.098, and 10.07 GHz. The minimum radius corresponds to the nominal external radius of the outer conductor (1.8 mm). The measured variation in the reflection coefficient closely follows the FDTD simulation, validating the computational tool.

Fig. 3(a) and (b) shows the calculated effects on the reflection coefficient of variations in the flange's radius, for a sensor immersed in water [Fig. 3(a)] and methanol [Fig. 3(b)] at 2.117, 5.098, and 10.07 GHz. The vertical axes of the figures indicate the percent deviation of the reflection coefficient from that of a probe with an infinite flange. Unlike the flange radius, changes in the flange thickness had little effect on the reflection coefficient for the three cases tested (0.25, 0.5, and 1 mm), as the only effect of thickness variation is to slightly shift the location of a scattering point distant

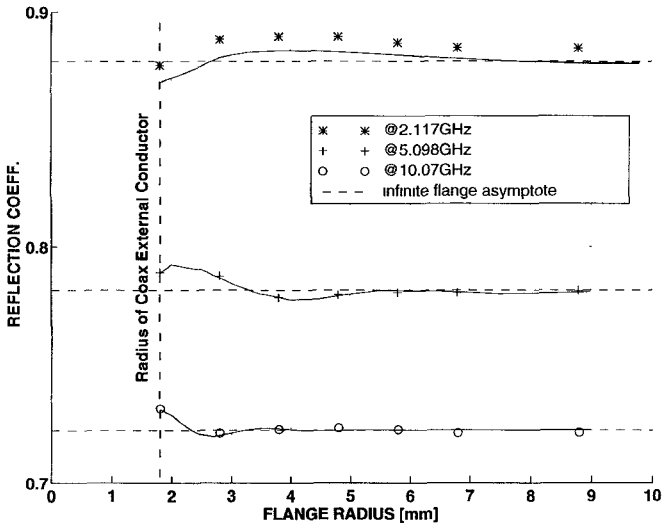

Fig. 2. Experimental and numerical (FDTD) results for water at 22°C.

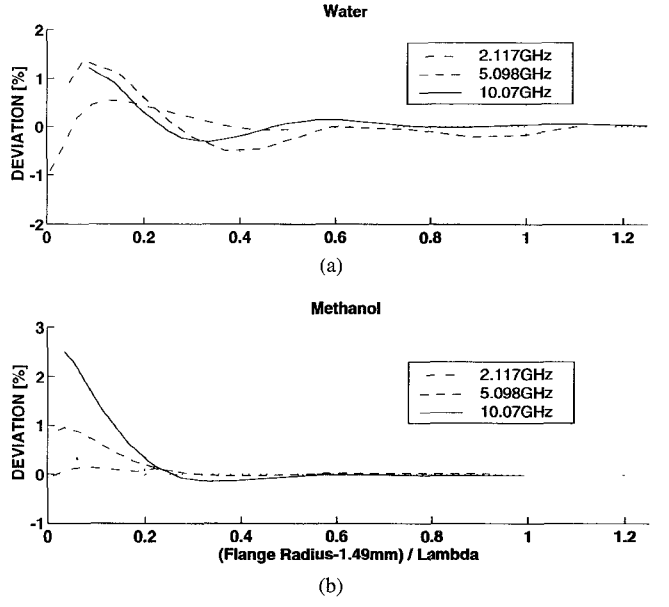

Fig. 3. Effects of flange radius on reflection coefficient. Note: 1.49 mm is the radius of the external conductor of the coaxial line. The thickness of the external conductor is the minimal flange size (a) water and (b) methanol.

from the aperture. For the cases examined, the reflection coefficient had a damped oscillatory dependence on the flange radius. For flanges with diameters of more than one half wavelength in the external dielectric, the reflection coefficient is within 0.25% of the infinite case.

Table II shows the change in the reflection coefficient of a sensor immersed in water and methanol with respect to variations in the inner and outer conductor inner radii at 2.117, 5.098, and 10.07 GHz. For the cases examined, the upper limit of the sensitivity (in percent per percent) of the reflection coefficient to changes in the inner conductor radius was 3.47. For changes in the outer conductor inner radius, the maximum sensitivity was 3.52. The sensitivities were calculated from measured data points [11]. For methanol, the reflection coefficient decreased with an increase in the inner or outer conductor inner radius. For water the reflection coefficient increased with an increase in the inner conductor radius but decreased with an increase in the outer conductor inner radius.

TABLE II
SENSITIVITY OF THE SENSOR TO THE CHANGES IN INNER (S_{in}) AND OUTER (S_{out}) CONDUCTOR RADII. $S_{in} = (r_{in}/|\Gamma|)(\partial/\partial r_{in})|\Gamma|$; $S_{out} = (r_{out}/|\Gamma|)(\partial/\partial r_{out})|\Gamma|$. r_{in}, r_{out} ARE, RESPECTIVELY, INNER AND OUTER RADII OF THE COAXIAL LINE

Material	Freq. [GHz]	S_{in}	S_{out}
Water	2.117	+0.224	+0.061
	5.098	+0.140	-0.192
	10.07	+0.140	-0.163
Methanol	2.117	-3.41	-1.38
	5.098	-3.47	-3.52
	10.07	-2.77	-2.17

IV. CONCLUSION

An open-ended dielectric sensor immersed in water and methanol was simulated using FDTD to investigate the dependence of the reflection coefficient on variations in the sensor geometry. Previously obtained moment method results were duplicated. Simulations with various flange configurations and perturbations in conductor radii indicated that the results from an unmodified open-ended coaxial line did not agree with those obtained using a numerical model in which the presence of an infinite flange or ground plane was assumed. The sensitivity of the reflection coefficient to changes in the conductor radii was as high a 3.5. These results show the need for numerical models incorporating the entire geometry of the line in order to obtain accurate inversion formulas.

REFERENCES

[1] J. M. Anderson, C. L. Sibbald, and S. S. Stuchly, "Dielectric measurements using a rational function model," *IEEE Trans. Microwave Theory Tech.*, vol. 42, pp. 199–204, Feb. 1994.

[2] D. Misra, M. Chabbra, B. R. Epstein, M. Mirotznik, and K. R. Foster, "Noninvasive electrical characterization of materials at microwave frequencies using an open-ended coaxial line: Test of an improved calibration technique," *IEEE Trans. Microwave Theory Tech.*, vol. 38, pp. 8–14, Jan. 1990.

[3] A. Nyshadham, C. L. Sibbald, and S. S. Stuchly, "Permittivity measurements using open-ended sensors and reference liquid calibration—An uncertainty analysis," *IEEE Trans. Microwave Theory Tech.*, vol. 40, pp. 305–314, Feb. 1992.

[4] C. L. Sibbald, "A new technique for modeling open-ended waveguide structures and its application to dielectric spectroscopy," Ph.D. thesis, University of Ottawa, Ottawa, Canada, Oct. 1991.

[5] C. L. Sibbald, S. S. Stuchly, and J. M. Anderson, "A new aperture admittance model for open-ended waveguides," *IEEE Trans. Microwave Theory Tech.*, vol. 42, pp. 192–198, Feb. 1994.

[6] K. S. Kunz and R. J. Luebbers, *The Finite Difference Time Domain Method for Electromagnetics*. Boca Raton: CRC, 1993.

[7] K. S. Yee, "Numerical solution of initial boundary-value problems involving Maxwell's equations in isotropic media," *IEEE Trans. Antennas Propagat.*, vol. AP-14, pp. 302–307, May 1966.

[8] W. K. Gwarek, T. Morawski, and C. Mroczkowski, "Application of the FD-TD method to the analysis of circuits described by the two-dimensional vector wave equation," *IEEE Trans. Microwave Theory Tech.*, vol. 41, pp. 311–317, Feb. 1993.

[9] J. G. Maloney, G. S. Smith, and W. R. Scott, Jr., "Accurate computation of the radiation from simple antennas using the finite-difference time-domain method," *IEEE Trans. Antennas Propagat.*, vol. 38, pp. 1059–1068, July 1990.

[10] P. J. Hum, M. S. Leong, P. S. Kooi, and T. S. Yeo, "(FD) 2-TD and experimental comparison for a cylindrical cavity loaded with lossy dielectric," *Microwave and Optical Technol. Lett.*, vol. 6, pp. 869–871, Dec. 1993.

[11] M. Okoniewski, J. Anderson, E. Okoniewska, and S. S. Stuchly, "Numerical analysis of the open-ended coaxial line radiating into the lossy and dispersive medium," in *IEEE Antennas Propagat. Soc. Int. Symp. Dig.*, Seattle, June 1994, vol. 3, pp. 1438–1441.

[12] G. Mur, "Absorbing boundary conditions for the finite-difference approximation of the time-domain electromagnetic-field equations," *IEEE Trans. Electromagn. Compat.*, vol. EMC-22, pp. 377–382, Nov. 1981.
[13] D. E. Merewether, "Transient currents induced on a metallic body of revolution by an electromagnetic pulse," *IEEE Trans. Electromagn. Compat.*, vol. EMC-13, pp. 41–44, May 1971.
[14] M. Okoniewski, J. Anderson, and S. S. Stuchly, "A technique to compute reflection coefficient in FDTD method," in *IEEE Antennas Propagat. Soc. Int. Symp. Dig.*, Seattle, June 1994, vol. 3, pp. 1446–1449.

Analysis of Anisotropic High Temperature Superconductor Planar Structures on Sapphire Anisotropic Substrates

Mohamed A. Megahed and Samir M. El-Ghazaly

***Abstract*—A full-wave finite-difference time-domain technique is used to study the anisotropy associated with high temperature superconductor (HTS) planar structures. The analysis is performed on anistropic YBCO film deposited on anisotropic sapphire substrate. The solution incorporates all the physical aspects of the HTS materials. The finite thickness of the anisotropic strip is rigorously modeled using a graded non uniform mesh generator. The propagation characteristics of HTS microstrip line are evaluated. The current distributions inside the HTS are calculated for both the normal and the super fluids. It is shown that the 90° r-cut sapphire substrate structure has lower loss and lower effective dielectric constant than the 0° r-cut substrate. Interesting aspects, concerning the anisotropy of HTS microwave structures, are presented.**

I. Introduction

The low surface resistance of superconducting materials is attractive for microwave and millimeter-wave applications such as antennas, filters, delay lines, interconnects, and microwave matching networks. The workhorse HTS materials are $YBa_2Cu_3O_x$, and TlBaCaCuO. They can be deposited on low dielectric loss substrate, such as Silica, Sapphire, Lithium Niobate, MgO, or LaAlO3, to form planar microwave structures. Although the sapphire substrate is anisotropic, the r-cut single crystal sapphire seems to be an appropriate substrate material for HTS applications. To exploit the exciting characteristics of HTS materials, accurate and flexible numerical models have to be developed.

The problem of calculating the propagation characteristics of isotropic superconducting microstrip line has been tackled before using different approaches [1], [2]. However, the field penetration effects is not rigorously modeled in many of those techniques. The finite thickness of the HTS strip need to be taken into consideration, especially when evaluating losses for the propagating wave inside the superconducting microstrip line [3]. Lee *et al.*, presented a full wave analysis that takes into account either the anisotropy in the HTS material or in the substrate itself, based on the spectral domain/volume integral equation approach (SDVIE) [4], [5].

In this paper, we present a technique for modeling a microstrip line incorporating an anisotropic superconducting material deposited on anisotropic sapphire substrate, based on the three-dimensional finite-difference time-domain method. The model incorporates all the physical aspects of the HTS through London's equations. The physical characteristics of the HTS are blended with the electromagnetic model using the phenomenological two fluid model. The complex propagation constant is calculated and the results are compared with the spectral domain technique. The effect of the anisotropy orientation on the characteristics of the microstrip line is studied. Also, effects of the anisotropy on the field distribution inside the structure is studied. This approach fits the needs for accurate computation of the dispersion characteristics of an anisotropic superconducting transmission line.

Manuscript received September 26, 1994; revised April 24, 1995. This work was supported by the National Science Foundation Grant ECS-9108933.

The authors are with the Department of Electrical Engineering, Arizona State University, Tempe, AZ 85287-5706 USA.

IEEE Log Number 9412672.

II. Anisotropic Superconductor Model

The two fluid model assumes that the electron gas in a superconductor material consists of two gases, the superconducting electron gas and the normal electron gas. The main parameters of the superconducting material are the London penetration depth λ_L and the normal conductivity σ_n. The total current density in superconducting material is expressed as follows:

$$\mathbf{J} = \mathbf{J}_n + \mathbf{J}_s \tag{1}$$

where $\mathbf{J}_n$ is the normal state current density. It obeys Ohm's law

$$\mathbf{J}_n = \sigma_n \mathbf{E}. \tag{2}$$

The superconducting fluid current density is obtained using London equation

$$\frac{\partial \mathbf{J}_s}{\partial t} = \frac{1}{\mu_o \lambda_L^2} \mathbf{E}. \tag{3}$$

These expressions are valid assuming that the HTS material is isotropic. However, experiments show that the properties of the HTS materials are anisotropic. Such anisotropy may have significant effects on the device performance. The designer is faced with several choices, such as the type of material and film direction, to obtain the optimum configuration that enhances the characteristics of the HTS material. A common feature of the family of HTS, including YBaCuO and TlBaCaCuO, is that they all have layered crystal structures. It is generally believed that the two-dimensional CuO_2 network is the most essential building block of the HTS materials. Thin-film transmission lines will favor films in which conducting sheets lie in the plane of the film. The anisotropy for the HTS can be represented by an anisotropic conductivity for the normal state, and an anisotropic London penetration depth for the superconducting state. The conductivity tensor $\overline{\sigma}$ is diagonal and is given by

$$\overline{\sigma} = \begin{bmatrix} \sigma_a & 0 & 0 \\ 0 & \sigma_b & 0 \\ 0 & 0 & \sigma_c \end{bmatrix}. \tag{4}$$

Also, the London penetration depth tensor $\overline{\lambda}$ is diagonal, and is written as

$$\overline{\lambda} = \begin{bmatrix} \lambda_a & 0 & 0 \\ 0 & \lambda_b & 0 \\ 0 & 0 & \lambda_c \end{bmatrix} \tag{5}$$

where a, b, and c are the principal axes of the anisotropic superconducting material. The normal conductivity and the London penetration depth in (1)–(3) will be replaced by their corresponding tensors to formulate the anisotropic superconductor model.